Computational features of numerical solution of non–stationary wave problems for an underground pipeline under seismic impacts

Karim Sultanov[1, a)], Sabida Ismoilova[1], and Nodirbek Akbarov[1]

[1]*Institute of Mechanics and Seismic Stability of Structures named after M.T. Urazbaev, Uzbekistan Academy of Sciences, Tashkent, Uzbekistan*

[a)] Corresponding author: sultanov.karim@mail.ru

Abstract. This article explores one–dimensional, nonstationary nonlinear wave problems involving an underground pipeline and the surrounding soil medium. The two systems are interconnected through conditions at their contact surface. Nonlinear laws that describe the variation of the friction force, which occurs in two stages, govern these conditions. In the initial stage, the friction force develops in response to relative displacement. In the second stage, the friction behavior conforms to the Amontons–Coulomb law. The numerical solution to this problem was obtained by employing the method of characteristics, followed by the finite difference method. During the process of obtaining numerical solutions, it was observed that the discretization steps in the computational domains on two conjugate characteristic planes significantly influence the stability of the results. This article discusses these computational features and other important aspects relevant to achieving a stable numerical solution for the "underground pipeline–soil medium" mechanical system. By establishing appropriate discretization steps, stable numerical solutions were successfully derived for the wave problems in question. The analysis of the numerical results indicated that when a low–frequency seismic wave propagates in soil, it generates soliton–like interaction waves with large amplitudes in the underground pipeline.

INTRODUCTION

The challenges associated with the seismic resistance of underground pipelines are often simplified to one–dimensional models [1–4]. In references [1] and [2], the pipeline is treated as a one–dimensional extended rod, which simplifies the analysis of its seismic resilience. References [3] and [4] consider the pipeline in conjunction with the surrounding soil medium, where the wave propagation problems for both the pipeline and the soil are addressed separately.

Non–stationary boundary value problems related to seismic wave propagation in soils are discussed in [5]. When a pipeline is situated within a soil medium experiencing a seismic load, the significantly greater deformation properties of the soil compared to those of the pipeline result in interaction forces at their contact surface. The longitudinal interaction laws between an underground pipeline and the surrounding soil are explored in [6], highlighting their notable nonlinearity due to the degradation of the soil contact layer under intense interaction [7]. The relevance of these laws to seismic resistance problems for underground pipelines is demonstrated in [4] and [7].

However, incorporating the external soil medium into the seismic resistance analysis for underground pipelines introduces complex coupled wave problems. This approach necessitates the simultaneous exploration of numerical solutions in two domains and their synchronization. This article focuses on the challenges of algorithm development and the achievement of stable numerical solutions for such non–stationary one–dimensional coupled nonlinear wave problems.

Numerous studies have been devoted to the wave processes in soils and numerical methods for solving wave problems for soils and underground pipelines were developed. The classical foundations of numerical methods and their practical application are presented in [8].

The three–dimensional numerical manifold method (3DNMM) has been further refined for mathematical modeling of wave propagation through homogeneous jointed rock masses, as discussed in [9]. To minimize the

negative impact of artificial boundaries, a viscous non–reflecting boundary is introduced to effectively absorb wave energy, thus enhancing the 3DNMM. Additionally, to model the elastic recovery properties of the infinite problem domain, a viscoelastic boundary, which evolves from the viscous non–reflecting boundary, is applied to improve the 3DNMM model.

Reference [10] focuses on a numerical method for computer modeling of wave propagation in three–dimensional dynamic loading problems for complex structures. This method utilizes a grid–characteristic approach that employs unstructured tetrahedral hierarchical meshes, multiple time steps, and high–order interpolation. By allowing the use of multiple time steps, the grid–characteristic method enhances performance and significantly reduces computation time.

In [11], an efficient method for modeling elastic wave propagation in unbounded domains is developed. It applies to soil–structure interaction problems involving scalar and vector waves, unbounded domains of arbitrary geometry, and anisotropic soil. A scalable boundary finite element method is used to derive a new equation for the unit impulse response matrix of displacement at the soil–structure interface. The proposed method is based on a piecewise linear approximation of the first derivative of the unit impulse response matrix of displacement and on the introduction of an extrapolation parameter to improve numerical stability. When combined, these two ideas allow the selection of significantly larger time steps compared to conventional methods, thus leading to higher efficiency.

In reference [12], the study aims to develop an efficient finite–difference scheme for solving direct seismic problems based on the equations governing the dynamics of elastic media in an axisymmetric formulation. For the numerical implementation of the scheme on multiprocessor computing systems, a two–cycle splitting method with respect to spatial variables was employed. During the splitting stages, one–dimensional systems of equations were decomposed into subsystems representing longitudinal, transverse, and torsional waves. This paper focused specifically on the case of longitudinal waves. A comparison was made between explicit grid–characteristic schemes and implicit predictor–corrector schemes with controlled energy dissipation, using exact solutions that describe traveling monochromatic waves.

In reference [13], traveling–wave solutions to the combined Korteweg–de Vries equation and a complex–coupled equation were obtained using the automatic Bäcklund transform method. The finite–difference method was utilized for the numerical approximation of the exact solutions. Additionally, these exact traveling–wave solutions were compared with the numerical solutions through tables and figures.

In reference [14], the Rayleigh wave velocity, a crucial parameter in ground motion analysis, was directly determined in an unconfined soil medium using numerical simulations with ABAQUS. The Rayleigh wave (R–wave) velocity was calculated from the displacement time history of a finite element model. Based on the results, a linear prediction equation for determining the R–wave velocity in soil was proposed. For this purpose, a two–dimensional finite element model was developed in conjunction with infinite elements at the boundary, subjected to dynamic loading. After confirming the presence of an R–wave in the soil medium through particle motion and verifying the displacement time history with analytical models, the R–wave velocity was determined using the positive peak vertical displacement of the particle.

Mathematical modeling of wave processes in soils is closely linked to examining how waves interact with structures within a soil medium. One of the most significant types of underground structures is trunk pipelines. A study referenced as [15] investigated the impact of dynamic behavior and lateral soil pressure on the dynamics of box culverts buried in dry, non–cohesive soils through numerical methods. This research explored how relative flexibility affects the dynamic displacements of the structure by varying both the dynamic shear modulus of the non–cohesive soil and the structural characteristics of the models. The study investigated shear strains, horizontal accelerations, wall deformations, and lateral dynamic soil pressures at various points of the culvert through numerical analysis. The findings from this numerical analysis were validated against results from a previous study that utilized centrifuge modeling. It was observed that the deformation patterns of the numerical models of the culverts align well with the data obtained from the centrifuge tests. The analysis revealed that dynamic lateral pressures acting on the sidewalls increase as the wall flexibility coefficient decreases. For a rigid prototype, the dynamic force on the sidewalls of a box culvert can be as much as 2.8 times the lateral soil load at rest. In contrast, for a flexible prototype, this dynamic force is only 1.6 times the static soil load [15].

In [16], a mathematical model was developed to assess the impact of seismic blast waves on a rock mass, particularly during the excavation process, using the principles of dynamic elasticity theory. An original finite–difference computational scheme was created for the numerical solution of this boundary value problem, employing the finite–difference method. The application of the splitting method to address a two–dimensional boundary value problem reduced the task to solving one–dimensional spatial differential equations. Additionally, efficient computational software was developed to implement the resulting numerical algorithm. Numerical solutions for the model problem are presented in the context of an elliptical excavation shape.

In [17], the challenge of accounting for highly uneven topography, inhomogeneities, and singularities in the ground domain is addressed. This consideration is essential for solving a variety of seismic problems, such as determining the locations of earthquakes. Therefore, employing a grid method that allows for a nonuniform distribution of grid nodes may be beneficial for modeling these issues. The longstanding use of finite–difference methods in modeling seismic wave propagation has enabled researchers to tackle this problem effectively. To validate the results, a numerical model was created using FLAC geotechnical software.

The review article [18] discusses the perfectly matched layer (PML) method and its various formulations that have been developed over the past 25 years for numerical modeling and simulating wave propagation in unbounded media. To enhance computational efficiency, the proposed time–domain formulation of the PML employs a hybrid approach. This combines a mixed (displacement–deformation) formulation for the PML domain with a classical (displacement–based) formulation for the physical domain of interest. The methodology utilizes the standard Galerkin finite element method (FEM) for spatial discretization, alongside a Newmark time–domain scheme paired with a finite difference (Crank–Nicolson) scheme for temporal discretization.

A brief analysis of studies [19] on the seismic interaction between soils and structures indicates that wave processes in soils and underground pipelines are being extensively researched worldwide. Most of the problems addressed in the literature are solved using numerical methods based on developed complex mathematical models that describe both one–dimensional and multidimensional motions of media and bodies.

An analysis of references [20–22] suggests that developing mathematical models to understand wave propagation in soils and their interaction with underground structures is a crucial first step. When dealing with nonlinear models, challenges may arise in obtaining accurate solutions to the problems being studied. Since numerical solutions are approximate, it is crucial to conduct thorough numerical experiments to ensure that the answers to these questions are reliable. Therefore, when constructing mathematical models and numerical solution algorithms, it is essential to consider all the specific features that may impact the results.

PROBLEM STATEMENT AND SOLUTION METHOD

The general problem of wave propagation in a soil medium, including an underground pipeline, is three–dimensional. However, solving such a problem numerically can lead to significant mathematical challenges. Therefore, as proposed in sources [1–3], we will use a simplified calculation method. In this approach, the soil and underground pipeline are modeled as a coaxial composite rod system, consisting of two layers along the radius.

In this model, the outer hollow rod represents the soil medium, while the inner rod represents the pipeline. Since we are focusing on a trunk pipeline, we assume its length is sufficiently large from the initial cross–section $x = 0$. The initial cross–section ($x = 0$, where x is the pipeline axis) is assumed to be a fixed cross–section of the soil and pipeline, where the seismic wave in the soil is set.

This calculation scheme significantly simplifies the original three–dimensional problem, reducing it to a one–dimensional model. This simplification, which is effective in studies [4, 20], retains the fundamental characteristics and essence of the wave propagation process within both the soil and the pipeline, despite the reduction in complexity.

This article examines a non–stationary wave process in a soil medium and an underground pipeline. While most studies on the seismic resistance of underground pipelines focus on stationary vibrations under seismic loads, it is well–known that during earthquakes, the vibrations of both buildings and structures, as well as underground pipelines, are non–stationary. Therefore, understanding the initial stages of underground pipeline vibrations under seismic loads is of significant interest. In light of this, the article poses and solves non–stationary boundary value problems related to the processes being considered.

The deformation laws for the soil and pipeline are assumed to be linear viscoelastic (a standard linear body):

$$\frac{d\varepsilon_i}{\mathrm{dt}} + \mu_i \varepsilon_i = \frac{d\sigma_i}{E_{\mathrm{Di}}\mathrm{dt}} + \mu \frac{d\sigma_i}{\mathrm{iE_{Si}}}$$
$$\mu_i = E_{\mathrm{Di}}\, E_{\mathrm{Si}} / (E_{\mathrm{Di}} - E_{\mathrm{Si}})\eta_i \qquad (1)$$

Here and below, i=1.2. For i=1, the parameter values refer to the pipeline, and for i=2, to the soil.

In (1), σ– is the longitudinal stress, ε– is the longitudinal strain, t – is time, E_S– is the static modulus of elasticity, E_D – is the dynamic modulus of elasticity, μ– is the bulk viscosity parameter, η– is the bulk viscosity coefficient.

In [6], interaction laws were developed based on serial experiments on the interaction of underground structure elements with soil. The most adequate of these is the law developed based on a standard linear body in the following form:

for $\sigma_N > \sigma_N$, $0 \le u \le u$:

$$\frac{d\tau}{K_{\mathrm{xD}}(\sigma_N, I_S)\mathrm{dt}} + \mu_S(\sigma_N, I_S, \dot{u})\frac{\tau}{K_{\mathrm{xS}}(\sigma_N, I_S)} = \frac{\mathrm{du}}{\mathrm{dt}} + \mu_S(\sigma_N, I_S, \dot{u})u \tag{2}$$

for $\sigma_N > \sigma_N$, $u > u$:

$$\tau = c + f\sigma_N \tag{3}$$

for, $\sigma_N \leq \sigma_N$:

$$\tau = 0 \tag{4}$$

where τ– is the interaction (friction) force, u– is the relative displacement, $u=u_g–u_c$, u_g– is the absolute soil displacement, u_c– is the absolute pipeline displacement; $u*$– is the critical value of the relative displacement, upon reaching which the soil contact layer is completely destroyed; K_{xD} – is the variable dynamic soil stiffness coefficient (as $\dot{u} \to \infty$); K_{xS} – is the variable static soil stiffness coefficient (as $\dot{u} \to 0$); μ_S – is the variable parameter of soil shear viscosity; $\dot{u}=du/dt$– is the rate of relative displacement of the pipeline and soil; $I_S=u/u*$ – is the parameter characterizing the structural destruction of the soil contact layer, $0 \leq I_S \leq 1$, for I_S =0 is the soil contact layer when contact bonds between the outer surface of the pipeline and the soil are intact, and for I_S =1, this bond is completely destroyed; f_v– is the coefficient of internal friction of the soil; σ_N– is the stress normal to the outer surface of the pipeline; $^{*}_{N}$– is the ultimate tensile strength of the soil (from here on, compressive stresses are taken to be positive).

Specific types of variable coefficients included in equations (2) and their physical justifications are given in [4, 6]. Note that the above interaction laws (2) – (4), with the corresponding constitutive relations given in [4, 6], are nonlinear laws of interaction between an underground pipeline and the surrounding soil.

The equations for the longitudinal motion of the pipeline and soil along the x–axis, coinciding with the pipeline axis, are of the following form:

$$\begin{gathered} \rho_{0\,i}\partial\, v_i/\partial\, t - \partial\, \sigma_i/\partial\, x + \chi_i\sigma_{\tau\,i} = 0 \\ \partial\, v_i/\partial\, x - \partial\, \varepsilon_i/\partial\, t = 0 \end{gathered} \tag{5}$$

where v_i– is the particle velocity (mass velocity); σ_i, ε_i – are longitudinal stresses and strains; ρ_{0i}– is the initial density; $\chi_i=sign(v)$– for the rod, and $\chi_i=–sign(v)$– for soil; $v = v_2$ – is the soil particle velocity; σ_τ – is the reduced friction force acting per unit length of the rod.

The values of σ_τ for the pipeline and soil are determined from the following relationship:

$$\sigma_{\tau\,i} = 4D_{\mathrm{Hi}}\,\tau/(\,D_{\mathrm{Hi}}^2 - D_{\mathrm{Bi}}^2) \tag{6}$$

where τ – is the friction force (shear stress), determined from equations (2)–(4); D_{Hi} – are the outer diameters, and D_{Bi} – are the inner diameters of the pipeline and soil.

The solution to the problem is reduced to integrating the nonlinear system (5), closed by equations (1), separately for the pipeline (i = 1, an internal problem) and separately for the soil (i = 2, an external problem). This system is coupled by nonlinear conditions on the contact surface between the pipeline and the soil, which determine the laws of variation of the interaction force (friction) τ according to equations (2)–(4).

Boundary conditions are at x = 0, the load is specified as a sinusoidal wave at the initial cross–section of soil:

$$\begin{gathered} \sigma = \sigma_{\max}\sin(\pi t/T), 0 \leq t \leq \theta \\ \sigma = 0, t > \theta \end{gathered} \tag{7}$$

where T– is the half–period of the load, θ – is the duration of the load, σ_{max} – is the amplitude of the load, and σ – is the longitudinal stress acting along the x–axis.

The conditions at the wave fronts in the soil and pipeline are initially set to zero. The initial conditions for the problems are also zero.

Equations (5), closed by equation (1), are hyperbolic. They have real characteristics and characteristic relations. Solutions can be derived using these characteristic relations, which are represented as ordinary differential equations.

The most widely used method for obtaining numerical solutions to the system of wave equations represented by equations (5) and (1) is the finite difference method [8].

The two systems of equations (1) for the soil and (5) for the pipeline are coupled systems that are solved separately. In reference [22], a method for numerically solving similar hyperbolic wave equations was developed using the theory of characteristics and the Hartree calculation scheme. This method reduces the system of wave equations to ordinary differential equations by employing the method of characteristics, after which the finite difference method is applied implicitly to numerically solve these ordinary differential equations.

COMPUTATIONAL FEATURES OF OBTAINING NUMERICAL SOLUTIONS

The discretization domains, according to the method given in reference [22], on the characteristic plane *t, x* for the soil medium and the pipeline are shown in Fig. 1.

The main difference between the calculation schemes for the pipeline and soil is the space step value Δx_c. The time step values Δt for the soil and the pipeline are the same and common. While the time steps Δt are the same for both calculation schemes, the space steps differ by the ratio of the longitudinal wave velocities:

$$\Delta x_g = \Delta x_c \, C_{\text{og}}/C_{\text{oc}} \tag{8}$$

In this case, the space step for the soil Δx_g, according to (8), is smaller by the ratio of the longitudinal wave velocities C_{0g} / C_{0c} .

In Fig. 1, the spatial step for the pipeline is three times larger than that for the soil.

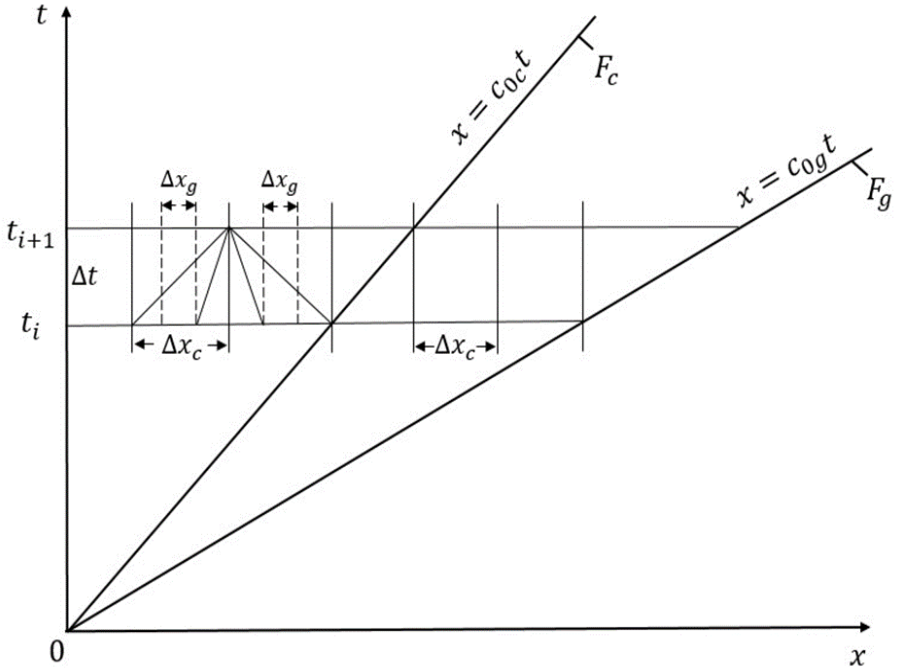

FIGURE 1. Domains of numerical solution for problems of wave propagation in soil and pipeline.

In Fig. 1, F_g– is the wave front in the soil; c_{0g}– is the longitudinal wave propagation velocity in the soil; Δx_g– is the discretization step in the soil along the *x*–axis; Δt– is the discretization step along the *t*–axis; t_{i+1} – is the upper, calculated time layer; t_i– is the lower, initial time layer; F_c – is the wave front in the pipeline; c_{0c} – is the longitudinal wave propagation velocity in the pipeline; Δx_c – is the discretization step along the x–axis for the pipeline.

Figure 1 shows two combined calculation schemes: the calculation schemes for the soil and the pipeline on the characteristic plane *t, x*. According to the Courant stability conditions, the characteristic must not extend beyond its cells for both the soil and the pipeline. This condition is satisfied here.

D.R. Hartree [22] proposed a calculation scheme illustrated in Fig. 1. The advantages of both the method of characteristics and the D.R. Hartree calculation scheme are discussed in detail in reference [22]. The core idea of this method is to seek the numerical solution within the fixed time layer t_{i+1}; the wave parameters in the time layer t_i are considered known. The spatial steps Δx_g and Δx_c are chosen such that the characteristic lines do not extend beyond the boundaries of a rectangular cell with sides Δt, Δx_g and Δt, Δx_c. The slope of the characteristic lines is determined by the wave propagation velocity in the soil and the pipeline.

The computational domain consists of the ordinate axis, where $x=0$, on one side, and the wave fronts in the pipeline F_c and soil F_g, on the other. This domain expands indefinitely between these two lines. As time *t* and spatial coordinates x increase, the computational domain continues to grow. Consequently, the number of discrete points in the computational time layer t_{i+1} for the soil and pipeline also increases over time. This demand for computational resources is substantial, as it requires significant power to perform the calculations. To address this issue, two approaches are employed. First, after filling the numerical arrays for the time layer, a “discharge” process is carried out. This involves eliminating data associated with individual discrete points in the time layer, allowing for further

calculations to be performed with doubled time steps Δt, Δx_g and Δx_c. While this procedure helps manage resource usage, it does result in some reduction in accuracy. Moreover, a sudden increase in the sampling steps Δt, Δx_g, Δx_c may cause abrupt changes ("jumps") in the wave parameters.

To avoid these artificial "jumps", which can lead to a slight decrease in wave parameters, it is essential to perform calculations with constant steps Δt, Δx_g, Δx_c throughout the entire process. This approach requires considerable computational resources, including processing speed and RAM. Calculating low–frequency wave parameters can sometimes take several hours. Therefore, it is necessary to limit these calculations to a single period or half–period. This limitation is further complicated when conducting parallel calculations for both the soil and the pipeline.

Figure 2 shows the types of calculation points on the calculation layer $t_i\ t_{i+1}$, on parallel planes tx. At $t = t_i$, all wave parameters and friction values are known. Calculation models are provided for cases where the longitudinal seismic wave propagation velocity in the pipeline is $C_{0c}=5000$ m/s, and in the soil, it is $C_{0g}=1000$ m/s. In this case $K_c=C_{0g} / C_{0c}=2$. The wave velocity in the pipeline is five times greater than in the soil. Other values and ratios of wave velocities in the pipeline and soil are also possible.

We convert to dimensionless variables and parameters using the following relationships (here, all parameters and quantities refer to the pipeline; for simplicity, their subscripts are omitted):

$$x^0 = \mu\ x/c_0\ ;\ t^0 = \mu\, x\ ;\ \sigma^0 = \sigma/\sigma_{\max}\ ;\ v^0 = v/v_{\max}\ ;$$
$$\varepsilon^0 = \varepsilon/\varepsilon_{\max}\ ;\ v_{\max} = -\sigma_{\max}/c_0\,\rho_0\ ;\ \varepsilon_{\max} = \sigma_{\max}/E_D\ ; \tag{9}$$

Using dimensionless variables and parameters (9), equations (1)–(8) are non–dimensionalized. Then, the dimensionless time Δt^0 and space Δx_c^0 steps for the pipeline become equal.

To obtain reliable numerical results, the solution domain is discretized based on the Courant stability condition:

$$\Delta x^0/\Delta t^0 \le 1 \tag{10}$$

In equation (10), Δx^0 is the dimensionless spatial discretization step, and Δt^0 is the dimensionless time discretization step. In Fig. 2 and further on, for simplicity, the superscripts are omitted.

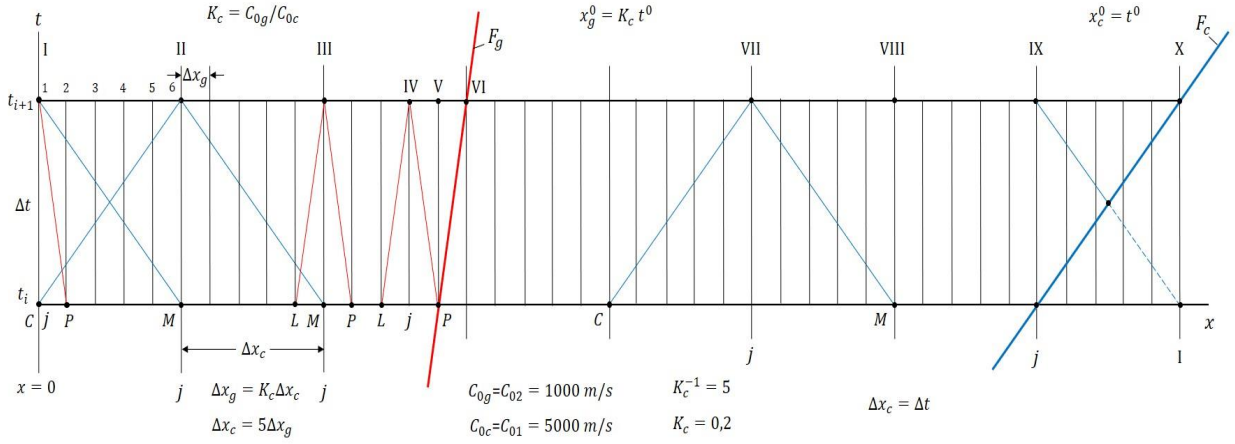

FIGURE 2. Typical discrete calculation points on the combined characteristic planes xt on the calculation time layer $t_{i+1}\ t_i$.

In Fig. 2, conditions (10) $\Delta x_c\ /\Delta t=1$ for the pipeline and $\Delta x_g\ /\Delta t=2$ for the soil ensure the stability of the numerical results.

In both cases, the characteristic lines do not extend beyond the computational cell with sides Δx_c , Δt for the pipeline and Δx_g , Δt for the soil.

When developing the algorithm for wave processes in the soil and pipelines, an important observation was made. The discretization step for the pipeline Δx_c is five times larger than that for the soil, Δx_g, i.e., $\Delta x_c\ /\ \Delta x_g=5$. Here, discrete point I at time t_{i+1} and point 1 coincide (Fig. 2). The next discrete points for the pipeline with the discretization step Δx_c, are points II, III…X. The wave parameters can be calculated separately for the pipeline and the soil, using the respective discretization steps. In this approach, the values of the wave parameters in the soil for points P and L are determined through linear interpolation between points C and M. Although this method significantly reduces computation time on the computer, it comes at the cost of degraded accuracy and stability, as will be demonstrated below.

Looking ahead, we observe that numerical experiments indicate that the wave parameters for the pipeline must also be determined at specific points in the soil, namely points 1, 2, 3, 4, 5, and 6, as illustrated in Fig. 2. In

numerical calculations, when we define the spatial step Δx_g for both the soil and the pipeline, the numerical solutions were found to be stable and smooth. However, this approach requires a significant amount of computational time.

Another issue arises when calculating the wave parameters in the pipeline at the initial points 2, 3, 4, and 5, which must be determined using a separate algorithm. At these discrete points, the left characteristic line for the pipeline extends beyond the initial cross–section $x=0$. To address this problem, we utilize a linear interpolation method. Specifically, the wave parameters in the pipeline for initial points 2, 3, 4, and 5, located between points I and II (as shown in Fig. 4), are determined through linear interpolation between discrete points 1 and 6. The calculation of the wave parameters in the pipeline using the general algorithm commences after the calculations at point 1, from point 6, or from point II (as shown in Fig. 2)

Therefore, numerical calculations of the wave parameters at time t_{i+1} for both the soil and the pipeline are modeled with the discrete spatial step Δx_g. The time step is taken $\Delta t = \Delta x_c = 5\,\Delta x_g$ for $K_c = C_{0g} / C_{0l} = 0.2$., and in other cases

$$\Delta t = K_c^{-1} \Delta x_g .$$

Calculations for discrete points of the pipeline using the above algorithm can be continued up to point III for the case where the points are arranged as in Fig. 2. Already at point III, the right characteristic line for the pipeline extends beyond the wave front line F_g. Calculations of the soil wave parameters can be carried out up to discrete point IV. At point V, the soil characteristic line already intersects the front line F_g in soil. Therefore, the soil wave parameters and interaction forces for point V are determined by linear interpolation between points IV and VI. Discrete point VI lies on the soil wave front, where all wave parameters are zero, since this front represents the lines of weak discontinuity.

Since the front line F_g is a weak discontinuity line, calculations of the wave parameters in the pipeline can be performed using a "through" calculation up to point VIII in Fig. 2. However, when the front line F_g is not a weak discontinuity line, this cannot be done. In this case, the wave parameters in the pipeline are also calculated taking into account the wave front in the soil. Calculations from point IX to point X are performed by interpolation. In this segment, the right–hand characteristic for the pipeline intersects the wave front line F_g in the pipeline. After the wave front F_g propagates in the pipeline, all soil particles are practically at rest. The equations for the wave front lines in the soil and the pipeline in dimensionless form are $\Delta x_g = K_c t$ and $\Delta x_c = t$, respectively.

Another feature of the algorithm is the calculation of points between the fronts F_g and F_c. It is important to note that the longitudinal seismic wave acts only in the soil and is initiated by the wave load at section $x=0$. This load does not act at this section of the pipeline, i.e., the initial section of the pipeline is load–free. A wave in the pipeline is generated solely by the interaction force (friction) that arises at the interface between the pipeline and the soil, specifically at the soil contact layer. Because the soil deforms more significantly than the pipeline, the friction force in the pipeline section from $x=0$ to the wave front F_g in the soil acts as an active force, prompting the pipeline to move. As a result, this movement generates waves within the pipeline, leading to the development of stresses, strains, and other related effects.

Behind the wave front F_g, a wave propagates through the pipeline. For this wave, the frictional force acts as a drag force (passive force), since there is no movement in the soil. Therefore, the wave in the pipeline behind the front F_g is quite weak. This same wave can generate a corresponding wave in the soil. However, as the calculation results show, it is practically zero. Based on numerical experiments, it was established that the main wave in the pipeline occurs from the initial section $x=0$ to the wave front in the soil F_g. In sections F_g F_c, where the soil is undisturbed, as will be shown below, significant stresses and strains do not occur in the pipeline.

Thus, taking into account the above features, resolving equations, and, based on them, algorithms for calculating the parameters of waves in the soil and pipeline were developed.

Soil characteristics are:

$\gamma_{0g} = 20$ kN/m^3 – specific gravity of soil;

$D_{Ng} = 3$ m – nominal outer diameter of the soil cylinder;

$D_{Bg} = 0.15$ m – nominal inner diameter of the soil cylinder;

$K_\sigma = 0.3$ – lateral soil pressure coefficient;

$\gamma_g = \gamma_2 = E_{Dg} / E_{Sg} = 2$– dimensionless quantity;

$C_{0g} = 1000$ m/s – longitudinal wave propagation velocity in soil;

$C_{gS} = 500$ m/s – transverse wave propagation velocity in soil.

Steel pipeline characteristics are:

$\gamma_{0c} = 78$ kN/m^3 – specific gravity of the pipeline material;

$D_{Nc} = 0.15$ m – outer diameter of the pipeline;

$D_{Bc} = 0.14$ m – inner diameter of the pipeline;

$\gamma_c=\gamma_1=E_{Dc}/E_{Sc}$=1.02– dimensionless quantity;

C_{0c} =5000 m/s – longitudinal wave velocity in the pipeline;

H_1=1.425 m – laying depth of the pipeline in soil;

μ_c=10000 s^{-1} – steel viscosity parameter;

L_c =107 m – nominal pipeline length.

Characteristics of the soil contact layer and pipeline–soil interaction are:

f_v=0.3 – coefficient of internal friction of soil;

C_v =10 kN/m^2 – soil cohesion coefficient;

u_*=10–3 m – relative displacement value at which the interaction process transitions to the Coulomb friction stage;

α=1.5 – dimensionless coefficient in formula (9);

χ=0.1 – dimensionless exponent in formula (11);

$\gamma_{vN}=K_{xDN}/K_{xSN}$=2– dimensionless quantity;

$\gamma_{v*}=K^*_{xD}/K^*_{xS}$ =4– dimensionless quantity.

Load characteristics are:

σ_{max}=0.7 MPa – longitudinal wave amplitude;

T= 10 s – half–period of a low–frequency longitudinal wave;

θ= 100 s – conventional duration of a longitudinal wave;

f= 1/2T=0.05 s–1 – frequency of a longitudinal wave in soil.

With these initial data, the frequency of longitudinal seismic waves is f= 1/2T=0.05 s^{-1}. This is a low–frequency wave. However, computer implementation and obtaining a numerical solution encounter the greatest difficulties for low–frequency seismic waves.

The above initial data are basic. If they are subsequently changed, this is noted separately.

In addition to the above initial data, the most important parameters of the numerical solutions are the discretization steps Δt, Δx_g and Δx_c in the solution domain on the characteristic plane tx.

Naturally, the accuracy and stability of the numerical solutions depend on the value of these discretization steps. Based on the analysis of numerical solutions of wave problems on the propagation of longitudinal waves in soils [5], the dimensionless time step is Δt^0 = 0.1; 0.05, or 0.01. This corresponds for μ_c=104 s^{-1} to dimensional times $\Delta t = \Delta t^0/\mu_c$ =10–5 s; 5*10–6 s, and 10–6 s. Then, for one half–period of the wave T=10 s, which corresponds to dimensionless time t^0=105, the number of discrete points is $n=T/\Delta t$=106. For Δt^0=0.01, which in the dimensional case is Δt =10–6 s, and n=107 along the t–axis. For Δt^0= 0.05, Δt = 5*10–6; n=2*106.

In the spatial coordinate x, the discretization steps are Δx_c^0=0.01 and Δx_c^0=0.1 for Δt^0= 0.1. For Δt^0=0.01, Δx_g^0= 0.001 and Δx_g^0=0.01.

In dimensional values, they take the following values: Δx_c =0.05 m for Δx^0=0.1 and Δx_c =0.005 mm for Δx_c^0=0.01. In these cases, the number of discrete points along the t^0–axis and along the Δx_c^0–axis are the same and are n=106 for Δx^0=0.1 and n=107 for x_c^0=0.01, respectively.

During the action time T= 10 s, the half–period of a longitudinal seismic wave for x_c^0 = 0.1, the wave travels a dimensionless distance $x_c^0=\Delta x_c^0 \cdot n=0.1\cdot 10^6=10^5$ along the pipeline. In soil, it is $x_c^0=K_c\cdot t_0^0=0.2\cdot 10^5=2\cdot 10^4$. In dimensional values, they are x_c=50000 m and x_g=10000 m.

Thus, for dimensionless Δt = 0.1 and Δx_c = 0.1; Δx_g =0.01, the values of t^0=105; x_c^0=105 and $x_g^0=2\cdot 10^4$ are dimensionless.

If the dimensionless sampling steps are taken ten times smaller, i.e., Δt^0=0.01; x_c^0=0.01; x_g^0=0.001, the number of discrete points in the half–period of the seismic longitudinal wave reaches 107 points; 107 points in the pipeline, and $n_g=2\cdot 10^7$ of discrete points in the soil.

As noted above, pipeline calculations are performed using discrete points in the soil, and the number of computational points in the pipeline is also $2\cdot 10^7$. These data demonstrate the resources required to perform numerical calculations of wave processes in the soil and pipeline on two superimposed parallel characteristic planes tx. The computational domains in plane tx expand during wave propagation, and the number of discrete points in the computational time layer t_{i+1} increases. Computational experiments have shown that the sampling steps Δt^0= 0.05; x_c^0= 0.01, and x_g^0= 0.01 are the most optimal. Increasing their values leads to instability of the numerical solution, while a decrease in their values yields good, consistent results. However, the latter case requires a significant amount of computation time (10–15 hours) on modern, high–performance computers.

Therefore, in the case of low–frequency seismic waves, computer calculations were limited to one half–period of the waves propagating in soil.

Let us consider the calculation results. In the first calculation option, the dimensionless discretization steps were $\Delta t^0 = 0.1$; $x_c^0 = 0.1$; $x_g^0 = 0.01$.

Figure 3 shows the time profile of a longitudinal seismic wave in soil for the first half–period. Since the wave is low frequency, it propagates without attenuation, i.e., the wave amplitude remains unchanged σ_g=0.7 MPa for all considered cross–sections x=0; 5; 10; 15; 20; 25, and 30m from the initial cross–section (curves 1–7). The curve of changes $\sigma_g(t)$ in these sections, practically lies on a single curve (Fig. 3).

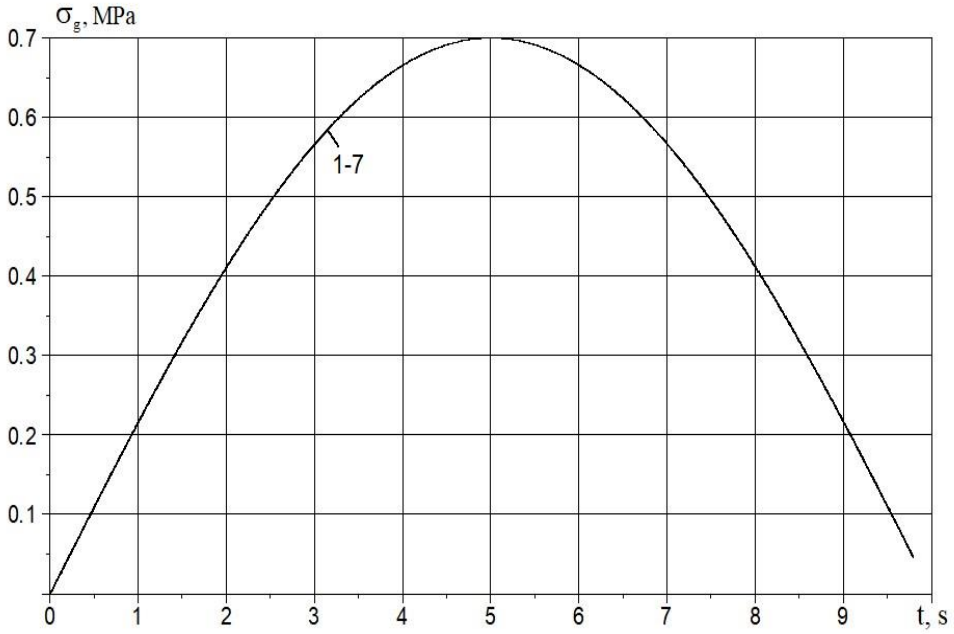

FIGURE 3. Half period of a seismic wave in soil with a frequency of f =0.05 s^{-1} at distances from the initial cross–section x= 0; 5; 10; 15; 20; 25; 30 m (curves 1–7)

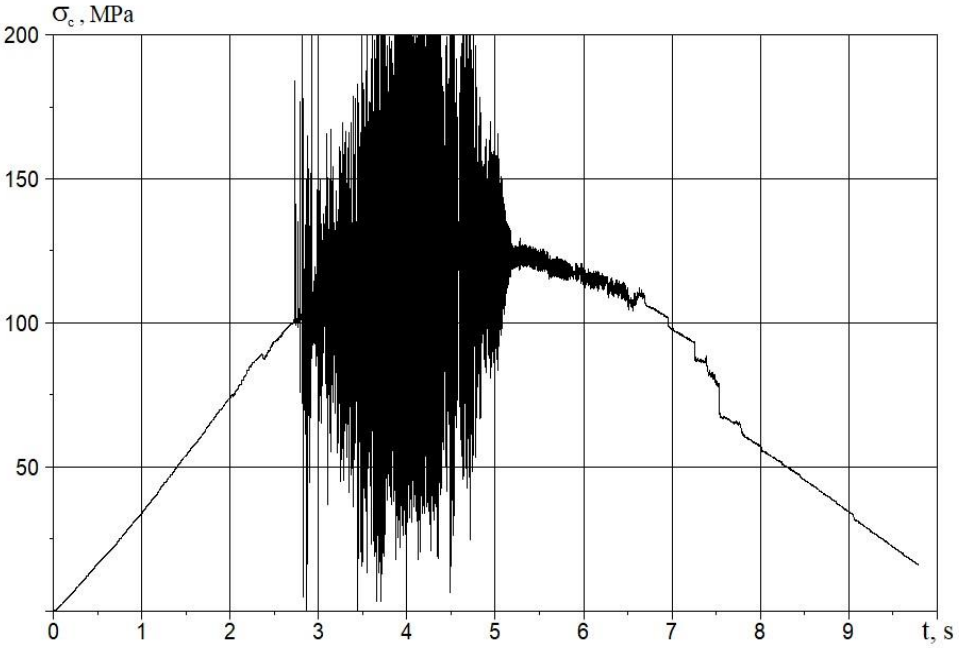

FIGURE 4. Changes in longitudinal stress over time in a pipeline at a cross–section of 5 m.

A completely different pattern is observed for a wave propagating along a pipeline. Figure 4 shows the wave profile over time for a pipeline cross–section of x=5 m. At the initial cross–section of the pipeline, x =0 m, according to boundary condition (7), no load is applied.

As seen from Fig. 7, the wave in the pipeline at x =5 m initially increases smoothly until x =2.8 sec. Then, strong instability in the stress value begins, lasting from 3 sec to 5 sec. The process then settles down again, and the stresses stabilize. The wave frequency remains virtually unchanged. The wave amplitude in the stability zones reaches

σ_c =125 MPa, which is significantly greater (by 178.6 times) than the wave amplitude in the soil (σ_g =0.7 MPa). This occurs due to the active behavior of the friction force at the pipeline–soil interface. In other words, the soil around the pipeline deforms significantly and "drags" the pipeline along with it, leading to the formation of high longitudinal stresses in the pipeline.

A similar pattern is observed at other cross–sections (x =10; 15; 20; 25, and 30 m) of the pipeline. Instability in longitudinal stress values in the pipeline occurs over time intervals from 3 sec to 5 sec. The amplitude of the wave in the pipeline decreases from σ_c =125 MPa at x =5 m to σ_c =115 MPa. In this case, the pipeline is considered elastic (γ_c =1.02), which prevents wave dissipation in the pipeline. Attenuation occurs due to the reduction in the active friction force on the outer surface of the pipeline.

The instability in stress values is linked to the variability of cross–sectional velocities within the pipeline. Figure 5 illustrates the changes in soil and pipeline cross–sectional velocities at x=0. The soil cross–sectional velocities vary smoothly from zero to a maximum of v_g =1.6 m/s and then gradually decrease (red curve in Fig. 5). This behavior can be attributed to the interaction force (an active frictional force), which has a negligible impact on the wave parameters in the soil. This is primarily due to the substantial nominal outer diameter of the soil (D_H=D_{Ng}=3 m), which is significantly larger by a factor of 20 than the outer diameter of the pipeline (D_H=D_{Nc}=0.15 m).

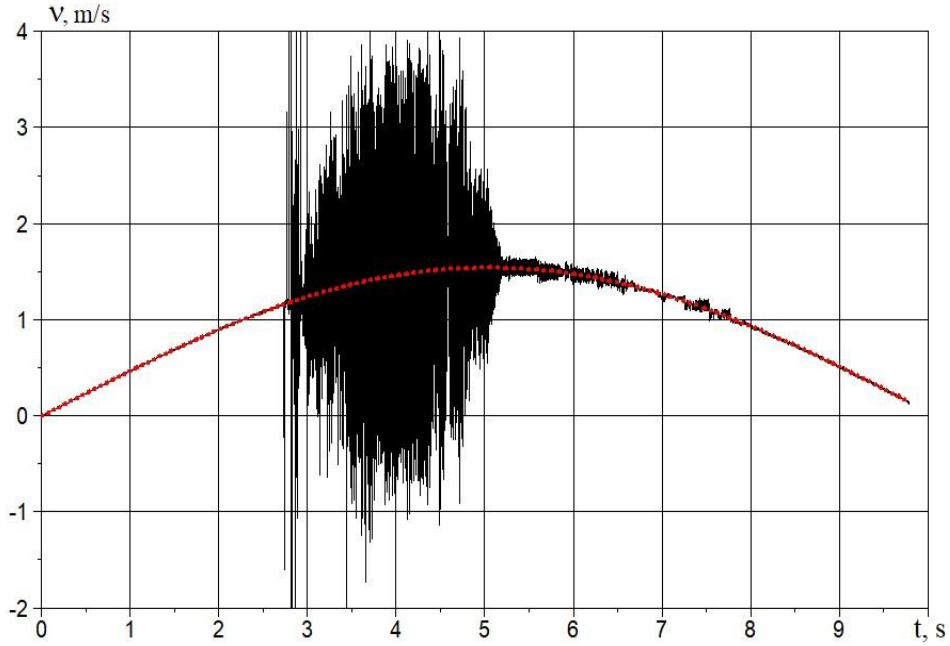

FIGURE 5. Changes in longitudinal cross–sectional velocities over time in the pipeline (black curve) and in the soil (red curve) at the initial cross–section x =0 m.

Instability in pipeline cross–sectional velocities, and consequently instability in relative velocities, leads to variability in shear stress values.

In [21], an exact analytical solution was obtained for the wave problem of shock wave propagation in embedded elastic rods, such as cages (holders). When the lengths of the rod and the cage (sleeve) are equal, as the wave propagates along them, after a certain time, the cross–sectional velocities of the rod and cage become equal. In [21], the rod and cage interact according to the Amontons–Coulomb law of dry friction.

In [20], a numerical solution was obtained for this problem in the case of viscoelastic rods and cages. Other laws of rod–cage interaction were also considered in [20]. In these cases, too, the velocities of the rod and cage cross sections become equal.

However, when solving these problems numerically, the velocities of the rod and cage cross–sections cannot be exactly equal. As a result, the relative velocity changes around zero with alternating signs. Consequently, the shear stress values also become alternating. As a result, we observe a loss of stability in the numerical solution results in the friction force values and dependencies, followed by a loss of stability in all other wave parameters of the underground pipeline.

In the second option, the discretization steps are $\Delta t^0 = 0.01$; $x_c^0 = 0.01$; $x_g^0 = 0.001$. In this case, they are an order of magnitude smaller than in the first option.

The longitudinal stresses in the soil remain unchanged, as in Fig. 3. The changes in longitudinal stresses in the second option in the pipeline cross–sections at x = 5; 10; 15; 20; 25, and 30 m (curves 1–6) are shown in Fig. 6. All curves of changes in longitudinal stresses 1–6 practically overlap each other. The maximum stress value is σ_{1max} =112 MPa, which is approximately the same as the result of the first option (Fig. 4). However, the results of the second option show virtually no instability or stress bifurcation.

Figure 7 shows the changes in the velocity of pipeline sections over time at x =0; 5; 10; 15; 20; 25, and 30 m (curves 1–7). The amplitude of the velocity change is virtually identical to the result of the first option in Fig. 5. The results of the second method show no instability.

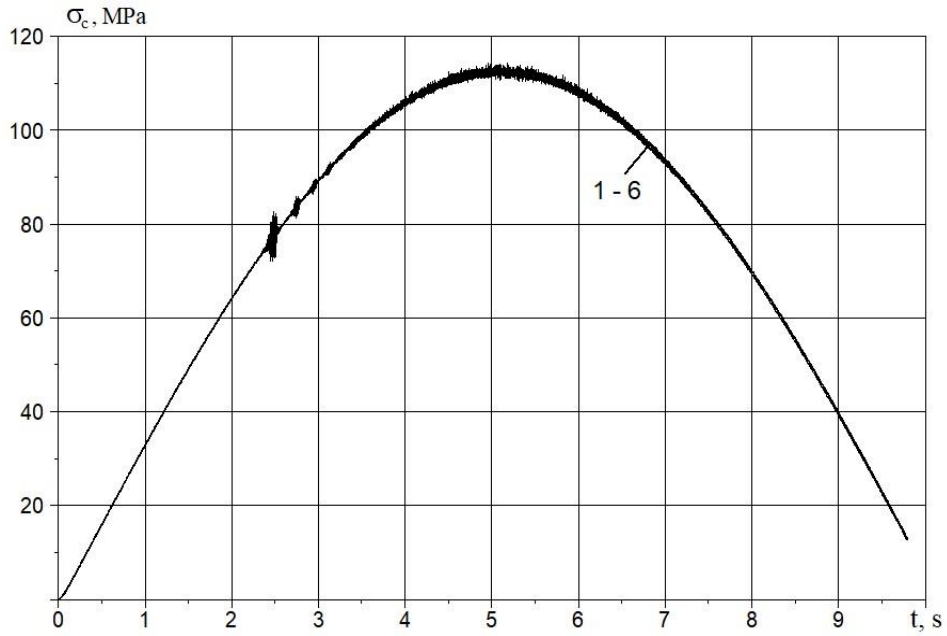

FIGURE 6. Changes in longitudinal cross–sectional velocities over time in the pipeline (black curve) and in the soil (red curve) at the initial cross–section x =0 m.

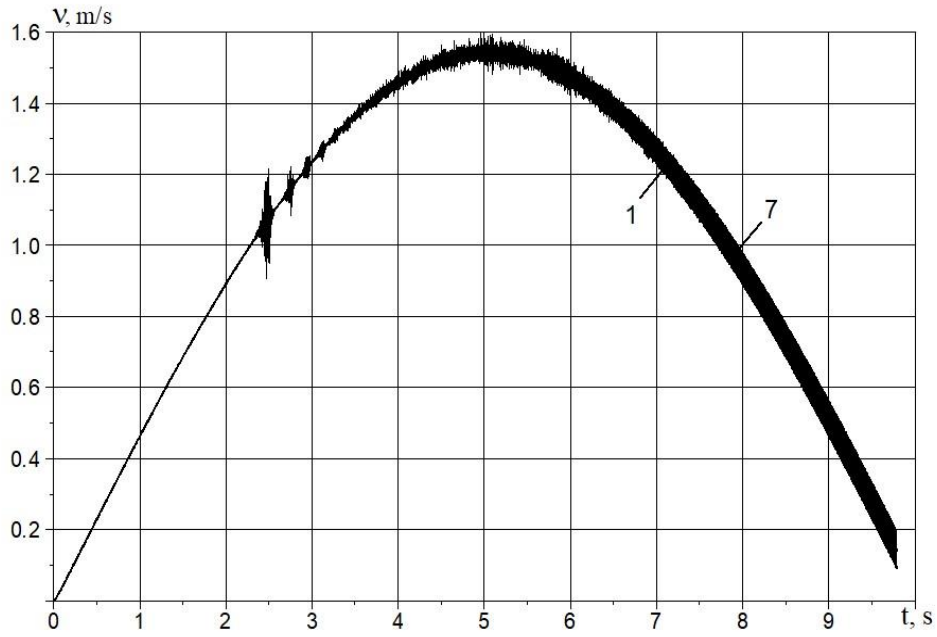

FIGURE 7. Velocity changes over time in pipeline cross–sections at x = 0; 5; 10; 15; 20; 25, and 30 m (curves 1–7).

However, note that as the seismic wave amplitude in the soil decreases, for example, at σ_{max} = 0.35 MPa, the instability of the wave parameters in the pipeline increases.

In the third option, calculations were performed with discrete steps x_c^0= 0.01; x_g^0= 0.01; Δt^0= 0.05. The amplitude of the longitudinal seismic wave in the soil was taken in dimensional form σ_{max} =0.35 MPa.

The values of other initial parameters remained unchanged.

In this case, the pattern of change in the longitudinal stress wave in the soil over time is similar to the one in Fig. 3, with the only difference being that the stress amplitude is σ_{gmax} =0.35 MPa.

Changes in longitudinal stresses in pipeline cross–sections at x=0; 5; 10; 15; 20; 25, and 30 m (curves 1–7) are shown in Fig. 8.

As can be seen from Fig. 8, the resulting numerical dependences $\sigma_c(t)$ are completely smooth, and no instability or bifurcations are observed.

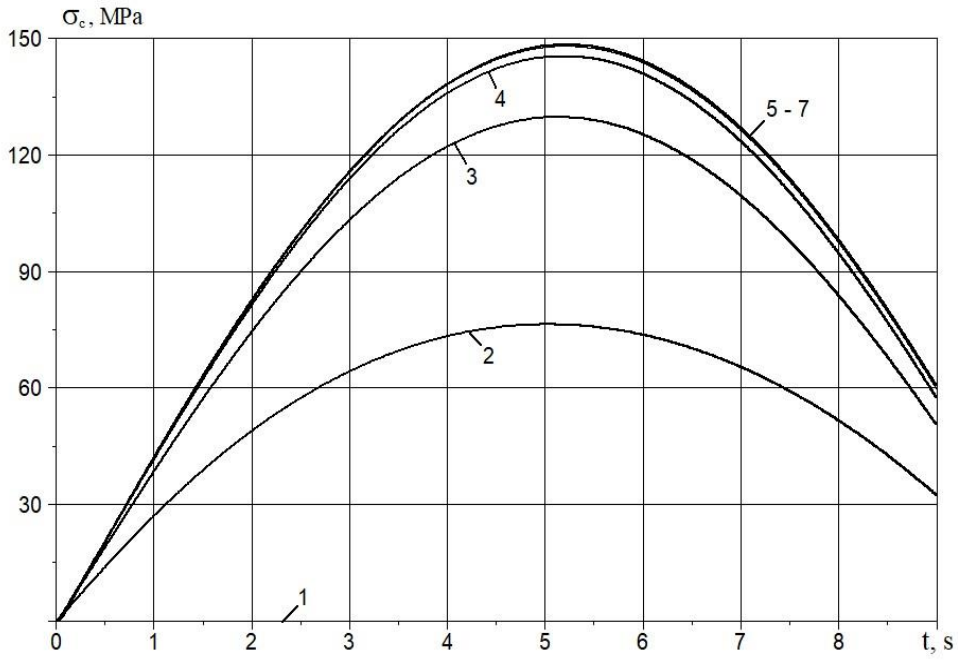

FIGURE 8. Changes in longitudinal stresses over time in pipeline cross–sections at x = 5; 10; 15; 20; 25 and 30 m (curves 1–7).

The longitudinal stress in the pipeline reaches the maximum σ_{cmax} =148.2 MPa. This value exceeds the amplitude of the longitudinal stress in the soil (σ_{gmax} =0.35 MPa) by 423.4 times. This multiple excess is the result of the active frictional force (interaction) acting on the underground pipeline due to soil deformation in the longitudinal direction (along the pipeline axis). This maximum stress is reached gradually along the pipeline. At the initial cross–section of the pipeline, the load is unaffected, and the stress values are zero (line 1). At the next pipeline cross–sections at x= 5 m and 10 m (curves 2 and 3), the stress amplitude gradually increases and at x = 15 m, it practically reaches its maximum σ_{cmax} =148.2 MPa (curve 4). Further, in the pipeline cross–sections at x = 20, 25, and 30 meters, this stress amplitude σ_{cmax} = 148.2 MPa remains constant. A powerful wave with a high amplitude travels along the pipeline. Calculations indicate that the wave's propagation velocity along the pipeline is significantly lower than the speed of sound within it. This leads to the discovery of a new, soliton–like interaction wave that moves at a different velocity compared to conventional longitudinal waves in the absence of surrounding soil. The investigation of this wave's properties falls outside the scope of this study and will be addressed in future research.

Figure 9 shows the changes in (longitudinal) strains over time in the soil (curves 1^0–7^0) and the pipeline (curves 1–7) at x = 0; 5; 10; 15; 20; 25, and 30 m, respectively.

As can be seen from Fig. 9, the longitudinal strains in all soil sections are identical (curves 1^0–7^0). In the pipeline, these strains, like the stresses, gradually increase until they reach an asymptotic value, which then remains constant. Notably, the maximum longitudinal strain in the pipeline (amplitude) is more than double the strain amplitude observed in the soil.

It is known that the quasi–static theory of seismic resistance of underground pipelines [1, 20] is based on the hypothesis of equality of soil and pipeline strains under seismic impacts. As seen from Fig. 9, this hypothesis is not fulfilled. Nevertheless, the quasi–static theory is currently used as a basis for normative methods [20].

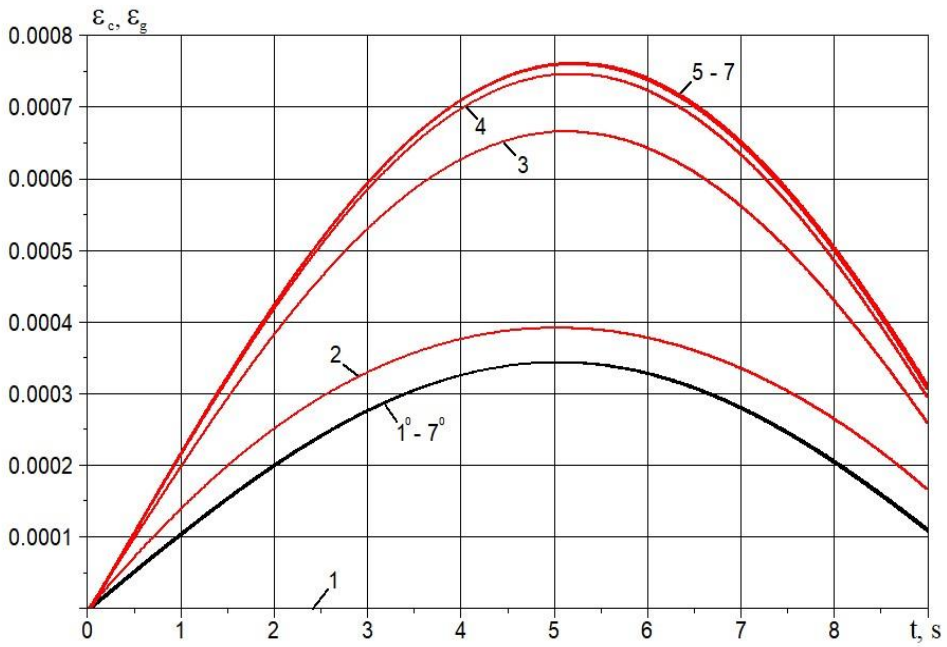

FIGURE 9. Changes in soil strains (curves 1^0–7^0) and pipeline (curves 1–7) over time at x = 0; 5; 10; 15; 20; 25, and 30 m.

Figure 10 shows changes in the velocity of soil particles (curves 1^0–7^0) and pipeline cross–sections (curves 1–7) over time at x= 0; 5; 10; 15; 20; 25, and 30 m. As seen from Fig. 10, the velocities of soil particles and pipeline cross–sections are almost identical. According to the changes in the relative velocity of the soil and pipeline v_t (Fig. 11), at x = 0, the maximum value of the relative velocity is v_{tmax} = 0.0021 m/s (curve 1). At x = 5 m, the values are v_{tmax} = 0.0004 m/s (curve 2), and at x = 10 m, v_{tmax} = 0.0002 m/s. In the remaining sections at x = 15 m; 20 m; 25 and 30 m (curves 4–7), the values of the relative velocity are practically zero.

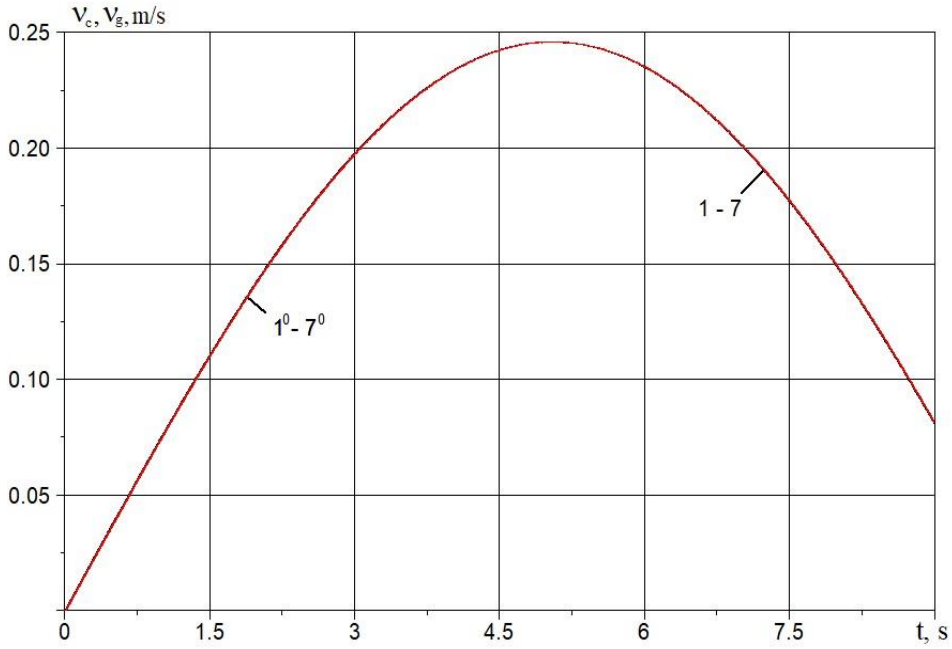

FIGURE 10. Changes in soil particle velocity (curves 1^0–7^0) and pipeline velocity (curves 1–7) over time in cross–sections at x = 0; 5; 10; 15; 20; 25, and 30 m.

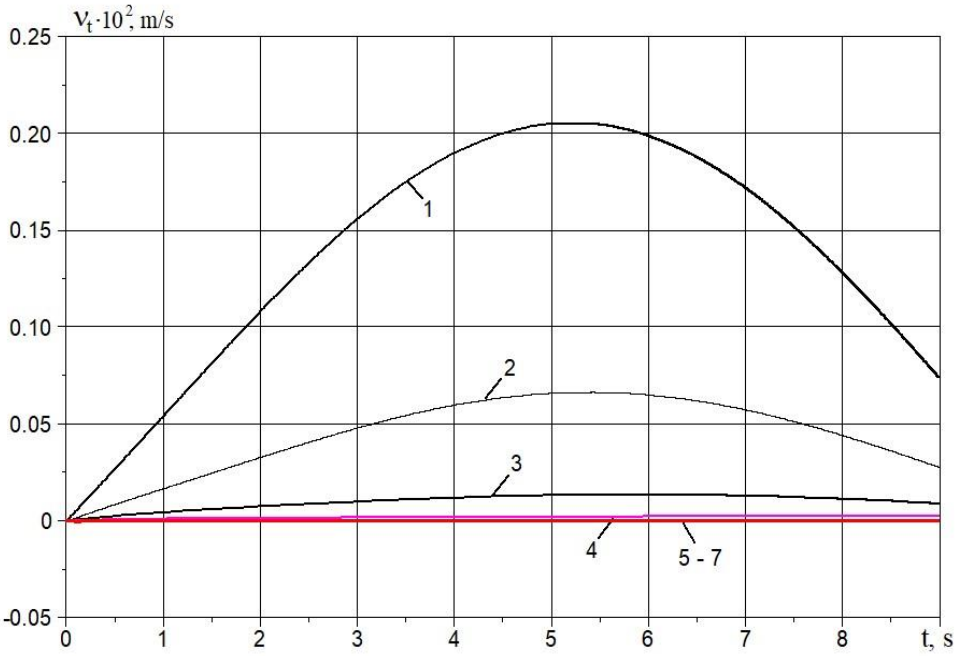

FIGURE 11. Changes in relative velocity over time in pipeline cross–sections at x = 0; 5; 10; 15; 20; 25, and 30 m (curves 1–7).

These results confirm that the soil and pipeline velocities ultimately become equal, as in [21].

CONCLUSIONS

The study focuses on the wave propagation process in a soil medium that contains an embedded underground pipeline, considering their interaction. Equations for the wave processes occurring in both the soil and the pipeline are defined and derived. Based on these equations, we develop an algorithm to numerically solve the wave problems using the method of characteristics and the finite difference method with an implicit calculation scheme.

The features of the developed numerical solution algorithm and methods to overcome them are determined. Based on the developed algorithm, a program for numerically solving the wave problems was developed in the FORTRAN–2005 algorithmic language. The program was implemented on a computer, and numerical experiments were used to determine the stability and reliability conditions for the resulting numerical solutions.

By conducting numerical experiments and analyzing the numerical solutions, the optimal discretization steps were determined in the solution domain on the characteristic plane tx for the soil medium and the underground pipeline.

It has been established for the first time that an active interaction force, specifically friction, can generate a soliton–like wave in an underground pipeline. This wave propagates through the pipeline without attenuation at a velocity lower than the speed of sound in the material of the pipeline.

Numerical calculations indicate that the assumption of equal longitudinal strains in both the soil and the pipeline, which underpins the standard quasi–static theory of underground pipelines, is not valid under the longitudinal action of a seismic wave.

ACKNOWLEDGMENTS

The work was conducted at the expense of the grant AL–8924073446 of the Agency for Innovative Development under the Ministry of Higher Education, Science, and Innovation of the Republic of Uzbekistan.

REFERENCES

1. M. J. O'Rourke and X. Liu, *Response of Buried Pipelines Subject to Earthquake Effects* (MCEER, Univ. at Buffalo, USA, 1999).

2. T. D. O'Rourke, J. K. Jung, and C. Argyrou, *Soil Dyn. Earthq. Eng.* **91**, 272–283 (2016). https://doi.org/10.1016/j.soildyn.2016.09.008
3. M. S. Israilov, *Mech. Solids* **58**, 26–37 (2023). https://doi.org/10.31857/S0572329922060083
4. K. S. Sultanov, *Facta Univ. Ser. Mech. Eng.* **22**, 485–501 (2024). https://doi.org/10.22190/FUME231227017S
5. K. S. Sultanov, *J. Appl. Math. Mech.* **66**, 115–122 (2002). https://doi.org/10.1016/S0021-8928(02)00015-1
6. K. S. Sultanov, *Int. Appl. Mech.* **29**, 217–223 (1993). https://doi.org/10.1007/BF00847001
7. A. A. Bakhodirov, S. I. Ismailova, and K. S. Sultanov, *J. Appl. Math. Mech.* **79**, 587–595 (2015). https://doi.org/10.1016/j.jappmathmech.2016.04.005
8. B. Alder, S. Fernbach, and V. Rotenberg, *Methods in Computational Physics*, Vol. 3 (Academic Press, New York and London, 1964).
9. Y. Yang, J. Li, and W. Wu, *Sci. China Tech. Sci.* **67**, 835–852 (2024). https://doi.org/10.1007/s11431-023-2517-8
10. I. B. Petrov, A. V. Favorskaya, N. I. Khokhlov, V. A. Miryakha, A. V. Sannikov, K. A. Beklemysheva, and V. I. Golubev, Radioelectron. Nanosyst. Inf. Technol. 7, 34 (2015). https://doi.org/10.17725/rensit.2015.07.034
11. X. Chen, C. Birk, and C. Song, Soil Dyn. Earthq. Eng. 65, 243–255 (2014). https://doi.org/10.1016/j.soildyn.2014.06.019
12. V. M. Sadovskii, O. V. Efimov, and E. A. Efimov, *J. Sib. Fed. Univ. Math. Phys.* **13**, 644–654 (2020). https://doi.org/10.17516/1997-1397-2020-13-5-644-654
13. A. Yokuş and D. Kaya, *Int. J. Mod. Phys. B* **34**, 2050282 (2020). https://doi.org/10.1142/S0217979220502823
14. K. S. Beena and M. N. Sandeep, *Indian Geotech. J.* (2021). https://doi.org/10.1007/s40098-021-00530-x
15. O. L. Ertugrul, *KSCE J. Civ. Eng.* **20**, 1737–1746 (2016). https://doi.org/10.1007/s12205-015-0235-1
16. A. P. Gospodarikov, Y. N. Vykhodtsev, and M. A. Zatsepin, *J. Min. Inst.* **224**, 405–414 (2017). https://doi.org/10.25515/pmi.2017.4.405
17. J. J. Benito, F. Ureña, E. Salete, A. Muelas, L. Gavete, and R. Galindo, *Soil Dyn. Earthq. Eng.* **79**, 190–198 (2015). https://doi.org/10.1016/j.soildyn.2015.09.012
18. F. Pled and C. Desceliers, *Arch. Comput. Methods Eng.* **29**, 471–518 (2022). https://doi.org/10.1007/s11831-021-09581-y
19. V. Anand and S. R. Satish Kumar, *Structures* **16**, 317–326 (2018). https://doi.org/10.1016/j.istruc.2018.10.009
20. K. S. Sultanov and N. I. Vatin, *Appl. Sci.* **11**, 1797 (2021). https://doi.org/10.3390/app11041797
21. L. V. Nikitin, *Statics and Dynamics of Rigid Bodies with External Friction* (Moscow Lyceum Publishing House, Moscow, 1998), 272 p.
22. N. E. Hoskin, in *Methods in Computational Physics*, Vol. 3, edited by B. Alder, S. Fernbach, and M. Rotenberg (Academic Press, New York and London, 1964), pp. 265–293.